Acta Crystallographica Section D
**Biological Crystallography**
ISSN 1399-0047

# Small-angle scattering gives direct structural information about a membrane protein inside a lipid environment

**Søren A. R. Kynde,[a] Nicholas Skar-Gislinge,[a] Martin Cramer Pedersen,[a] Søren Roi Midtgaard,[a,c] Jens Baek Simonsen,[a] Ralf Schweins,[b] Kell Mortensen[a] and Lise Arleth[a]***

[a]Structural Biophysics, Niels Bohr Institute, Faculty of Science, University of Copenhagen, Denmark, [b]Institute Laue–Langevin, Grenoble, France, and [c]Nano-Bio Science, Department of Chemistry, University of Copenhagen, Denmark

Correspondence e-mail: arleth@nbi.ku.dk

Received 5 June 2013
Accepted 15 October 2013

Monomeric bacteriorhodopsin (bR) reconstituted into POPC/POPG-containing nanodiscs was investigated by combined small-angle neutron and X-ray scattering. A novel hybrid approach to small-angle scattering data analysis was developed. In combination, these provided direct structural insight into membrane-protein localization in the nanodisc and into the protein–lipid interactions. It was found that bR is laterally decentred in the plane of the disc and is slightly tilted in the phospholipid bilayer. The thickness of the bilayer is reduced in response to the incorporation of bR. The observed tilt of bR is in good accordance with previously performed theoretical predictions and computer simulations based on the bR crystal structure. The result is a significant and essential step on the way to developing a general small-angle scattering-based method for determining the low-resolution structures of membrane proteins in physiologically relevant environments.

## 1. Introduction

Membrane proteins reside in the lipid membranes of the cell. They play a central role in transport and signalling across the cell membrane and are consequently key targets in drug development. The function of membrane proteins is closely coupled to their intrinsic flexibility. Furthermore, membrane proteins require a native membrane-like local environment in order to maintain structural and functional stability. These central features imply that despite the remarkable breakthroughs in the last few years (Morth *et al.*, 2007; Rosenbaum *et al.*, 2009), it is still regarded as extraordinarily challenging to crystallize membrane proteins to obtain high-resolution structural information. Consequently, only 406 structures[1] out of roughly 36 000 unique protein structures[2] published in the Protein Data Bank correspond to membrane-protein structures. This should be seen in light of the fact that more than 26% of the proteins coded for by the human genome are expected to be membrane proteins (Wallin & von Heijne, 1998; Fagerberg *et al.*, 2010).

The function of membrane proteins takes place in close interplay with the surrounding membrane environment. As a result of the disordered nature of lipids and the often rather extreme conditions of membrane-protein crystallization, little information about the structural interplay between membrane proteins and the surrounding fluid lipid environment is

[1] According to a search in the database of membrane-protein structures maintained by Stephen White as of 1 June 2013, counting only entries solved by diffraction methods (http://blanco.biomol.uci.edu).
[2] According to a search of the Protein Data Bank on 1 June 2013, counting only entries solved by diffraction methods and removing similar sequences at 100% identity (http://www.rcsb.org/pdb/search/advSearch.do).

obtained from crystallographic data (Sonntag *et al.*, 2011; Gonen *et al.*, 2005). This means that while numerous theoretical predictions and computer simulations (Lomize *et al.*, 2011; Sonntag *et al.*, 2011) have been made of the interactions between membrane proteins and lipid membranes, very little directly experimentally obtained structural information is available to guide these simulations and theory development.

Nanodiscs are small lipoprotein complexes containing a small sheet of phospholipid bilayer stabilized by two amphipathic membrane scaffolding proteins (MSPs) spanning the rim of the phospholipid sheet. Numerous experimental studies have exploited the fact that membrane proteins can be embedded into the phospholipid interior of the nanodisc (Frauenfeld *et al.*, 2011; Bayburt & Sligar, 2003; Yao *et al.*, 2009; Whorton *et al.*, 2007; El Moustaine *et al.*, 2012) and have used the platform to enable functional studies of membrane proteins in solution-like conditions. While solution studies are also regularly performed on membrane proteins reconstituted into detergent micelles, the nanodisc system has proved to have superior properties with respect to maintaining the function of the membrane proteins (Lyukmanova *et al.*, 2012; Berthaud *et al.*, 2012; Calcutta *et al.*, 2012).

In a recent study, a combination of small-angle X-ray and neutron scattering (SAXS and SANS) allowed us to demonstrate that the unloaded nanodiscs are remarkable structurally homogeneous (Skar-Gislinge *et al.*, 2010; Skar-Gislinge & Arleth, 2010), particularly compared with detergent micelles, where the size typically follows a broad size distribution. This structural homogeneity of the nanodisc is most likely to be an effect of the balance between the rather fixed perimeter of the discs as imposed by the amphipathic MSP and the well defined preferred area per head group and hence molecular packing of the incorporated phospholipids. In the analysis of SAXS/SANS data, good structural homogeneity provides the possibility of obtaining high resolution in the structural interpretation. In the study mentioned above this fact allowed unprecedented insight into the nanodisc structure, including the lipid packing inside the discs.

The structural homogeneity of the nanodisc system, its size and its native membrane-like environment make it a promising platform for structural studies of membrane proteins. Interesting results have already been obtained using cryo-EM on a membrane-anchored protein system (Frauenfeld *et al.*, 2011), and the nanodisc platform was recently used in a very interesting NMR study of fully embedded transmembrane structures (Hagn *et al.*, 2013). Small-angle scattering is ideally suited to the solution-based nanodisc system and can even provide information about the phospholipid bilayer and on the interplay between lipids and membrane proteins, information that is neither available from cryo-EM owing to the low electron density of the lipids nor from NMR, where usually the lipids are deuterated to remove the signal. In this light, it is somewhat surprising that to date only a little new insight about membrane proteins inserted into nanodiscs has been obtained with SAXS/SANS.

To date, only a few examples of small-angle scattering studies of a membrane protein incorporated in a nanodisc are available in the literature, all of which are based on SAXS data. The studied proteins include a cytochrome P450-type membrane protein incorporated into a POPC-based nanodisc (Baas *et al.*, 2004), bacteriorhodopsin (bR) incorporated into DMPC-based nanodiscs (Bayburt *et al.*, 2006) and, most recently, the incorporation of a curdlan synthase into two different preparations of nanodiscs based on either POPC or *Escherichia coli* lipids (Periasamy *et al.*, 2013). Owing to the lack of adequate data-analysis methods, however, none of these studies exploit the full information content of the SAXS curves. The data treatment predominately consists of indirect Fourier transform (IFT) analysis, meaning that only the maximum dimensions of the particles can be determined and qualitative comparison with other systems can be made. However, without a model no information about the structure or the localization of the membrane protein into the nanodisc can be obtained. In one case (Baas *et al.*, 2004), an attempt to model the structure of the particle was made, but no fits to the data were shown. This means that the model is in agreement with the overall predicted size, but it is not demonstrated that the model complies with the entire measured scattering function. Including this valuable experimental constraint in the modelling process allows a lot more detail to be extracted, as will be demonstrated here.

In the present article, we report the successful reconstitution of bacteriorhodopsin into nanodiscs containing a 2:1 molar ratio of POPC and POPG. Using a combination of small-angle X-ray and neutron scattering (SAXS and SANS), we show that the vertical position of bR is slightly off-centred, with the C-terminus protruding more than the buried N-terminal region. This has been theoretically predicted (Lomize *et al.*, 2011), but has never been experimentally observed in a real membrane environment. We find that bR is indeed completely surrounded by lipids but is not confined to the centre of the plane of the disc. Furthermore, we observe a small but significant structural modulation of the surrounding phospholipid bilayer, including an increase in the phospholipid area per head group.

The central result of the article is, however, the development of a novel approach for analyzing scattering data from the combined system of nanodisc and membrane protein. We describe a model that is fully compatible with all prior knowledge of the system and with the scattering curves in two different contrast situations. The approach is directly applicable to any system of a membrane protein of well known structure that is embedded in a nanodisc.

## 2. Materials and methods

### 2.1. Sample preparation

**2.1.1. Bacteriorhodopsin purification**. Bacteriorhodopsin (bR) was produced and purified according to previously published reports (Oesterhelt & Stoeckenius, 1974; Dencher, 1982). Briefly, salt medium containing 250 g NaCl (Sigma), 20 g $MgSO_4.7H_2O$ (Sigma), 10 g peptone (Oxoid), 3 g trisodium citrate (Sigma) and 2 g KCl (Sigma) per litre of $H_2O$

was inoculated with *Halobacterium salinarium*. After 5–6 d of growth at 40°C illuminated with a 500 W lamp, the cells were pelleted and washed in salt buffer containing 250 g NaCl (Sigma), 20 g $MgSO_4.7H_2O$ (Sigma) and 2 g KCl (Sigma) per litre of $H_2O$. The cells were resuspended in 25 ml Milli-Q $H_2O$ per gram of cells. DNase (Sigma) was added and the solution was left stirring overnight at 4°C. Cell debris was spun down, the supernatant was transferred to centrifuge tubes and the membranes were pelleted at 54 000*g* for 1 h. The supernatant was discarded and the pellet was resuspended in Milli-Q $H_2O$ and spun down a further two times to remove impurities. Isolated membranes were resuspended in a minimum amount of Milli-Q $H_2O$ and carefully layered on top of a sucrose gradient consisting of a step gradient of 30, 40 and 50% sucrose dissolved in STED buffer consisting of 10 m*M* Tris–HCl pH 7.5, 1.5 m*M* EDTA, 0.5 m*M* DTT. The gradient was centrifuged overnight at 200 000*g* to reach equilibrium. The next day, the band containing the purple membrane was extracted and dialyzed against 25 m*M* phosphate buffer pH 7.4 to remove the sucrose. The purple membrane was diluted so that the detergent to bR weight ratio would be ∼20 when octyl glucoside (OG; Applichem) was added to a final concentration of 40 m*M*. The solution was lightly sonicated, left under gentle agitation at room temperature overnight and protected from light. After solubilization, the bR was loaded onto a Superdex 200 column (GE Healthcare) equilibrated in 25 m*M* phosphate buffer pH 7.4, 40 m*M* octyl glucoside. Fractions containing monomeric bR were collected, concentrated, flash-frozen and stored at −80°C until further use.

**2.1.2. Biotinylation of bR**. bR was biotinylated in order to facilitate the separation of bR-containing nanodiscs from unloaded nanodiscs by affinity purification. bR in 25 m*M* phosphate buffer pH 7.4 containing 40 m*M* octyl glucoside was mixed with a 25-fold excess of succinimidyl-6-(biotinamido)-6-hexanamido hexanoate (NHS-LC-LC-Biotin; Pierce) at 20°C for 1.5 h. The excess unreacted NHS-LC-LC-Biotin was diluted by adding OG–phosphate buffer to the bR solution and concentrating the sample using a 10 kDa cutoff spin filter (Amicon), resulting in a dilution of >5000. A biotinylated bR sample prepared under similar conditions was found to contain 1.6 biotin groups on average using a 2-hydroxyazobenzene-4-carboxylic acid/avidin assay (Green, 1970).

**2.1.3. MSP preparation**. The amphipathic membrane-scaffolding protein used in the present work was MSP1D1(−). MSP1D1 was expressed and purified according to previously published procedures (Ritchie *et al.*, 2009) and the His tag was cleaved off by adding TEV protease to the sample and utilizing the TEV site incorporated between the His tag and the MSP1D1 sequence. This produced the final MSP1D1(−) protein used in the samples.

**2.1.4. Reconstitution of bR into nanodiscs**. The preparation of nanodiscs with and without reconstituted bR is described in detail in Bayburt *et al.* (2002) and Bayburt & Sligar (2003), respectively. The molar ratio between MSP1D1(−) and bR was 10:1 in order to minimize the formation of reconstituted nanodiscs containing two or three molecules of bR. The stoichiometry between phospholipids and MSP1D1(−) was 67:1. We used a lipid composition of 2:1 POPC:POPG to form a lipid liquid-phase environment at room temperature and to introduce negatively charged lipids into the lipid bilayer in the nanodisc. These two bilayer features should facilitate a good mimic of the cell membrane compared with DMPC-based bR-nanodiscs. A lipid composition of 2:1 POPC:POPG was used for both the bR-reconstituted nanodisc and the unloaded (non-reconstituted) nanodisc preparations. MSP1D1(−) in 20 m*M* phosphate buffer, bR in OG–phosphate buffer and the lipid–OG–phosphate solutions were mixed. The mixture had a final lipid concentration of 10 m*M* and was incubated at 4°C for 1 h with stirring. SM-2 Bio-Beads (Bio-Rad) were added and the Bio-Bead mixture was stirred overnight at 4°C to remove the detergent. The bR-reconstituted nanodiscs were subsequently separated from the unloaded nanodiscs by affinity chromatography. An immobilized monomeric avidin resin (Pierce) was used according to the manufacturer's instructions. The purified bR-nanodisc sample was stored in a 15% glycerol Tris buffer solution flash-frozen in liquid nitrogen. Finally, the bR-nanodisc solution was thawed and purified using a Superdex 200 size-exclusion column (GE Healthcare) pre-equilibrated in buffer consisting of 20 m*M* Tris–HCl pH 7.4, 100 m*M* NaCl at 4°C. Fractions containing the sample were pooled and concentrated using a 50 kDa cutoff spin filter prior to the SAXS measurements. The buffer was exchanged to a $D_2O$-based buffer prior to the SANS measurements by diluting the sample ten times in $D_2O$ buffer and then concentrating the sample with a 50 kDa cutoff spin filter. The procedure was repeated four times to ensure almost complete exchange into $D_2O$ buffer.

The theoretical ratio between the absorbance at 280 and 550 nm of the MSP1D1(−)-based nanodisc with only one bR reconstituted into the disc is 2.8 according to UV–Vis studies conducted by Bayburt & Sligar (2003). The final bR-nanodisc used for the small-angle scattering measurements exhibited a ratio of 2.7 according to UV–Vis measurements. Thus, it was confirmed that the solution consists of bR-loaded nanodiscs with only a single bR molecule incorporated in each of the nanodiscs.

**2.1.5. Small-angle scattering**. For the bR-loaded discs, small-angle X-ray scattering experiments were performed on the BioSAXS beamline ID14-3 at the European Synchrotron Radiation Facility (ESRF), Grenoble, France. Data were collected at 20°C using the fixed instrument as described in Pernot *et al.* (2010). In Fig. 1(*a*) the data are shown as an absolute scaled intensity as a function of $q = 4\pi\sin(\theta)/\lambda$, where $2\theta$ is the scattering angle and $\lambda$ is the X-ray wavelength. Radial averaging and $q$-conversion of data were performed using the standard software at the beamline. Absolute scaling, *i.e.* expressing intensities as scattering cross-section per sample volume in units of $cm^{-1}$, was performed using BSA as a standard (Mylonas & Svergun, 2007).

The small-angle neutron scattering of the bR-loaded nanodiscs was performed on beamline D11 at the Institut Laue–Langevin, Grenoble, France (Lieutenant *et al.*, 2007). The close proximity to the SAXS facility enabled the measurement of the same sample preparations within a few

hours. In order to cover the desired $q$ range, measurements were performed at two sample-to-detector distances: 1.504 m with 4 m collimation for the $q$ range 0.0060–0.43 Å$^{-1}$ and 9.495 m with 10.5 m collimation for the $q$ range 0.0069–0.072 Å$^{-1}$. The wavelength spread, $\Delta\lambda/\lambda$, was 10% for all settings. Azimuthal integration of the data as well as absolute scaling with water as a standard were performed using the *LAMP* software package at the beamline. The data are shown in Fig. 1(*a*).

On another occasion, we performed SAXS and SANS measurements of the unloaded nanodiscs. These data are shown in Fig. 1(*c*). Again, the beamtimes were scheduled so that both measurements could be performed on the same sample preparation within 24 h.

SAXS measurements of the unloaded discs were performed on the BioSAXS beamline BM29 at ESRF. This is the same instrument as above but moved from beamline ID14-3 to BM29. The settings and data treatment were the same as described for the loaded nanodiscs above.

SANS measurements of the unloaded discs were performed at KWS 1, Forschungs Neuronenquelle Heinz Maier-Leibnitz, Munich (FRM II). Measurements were performed using

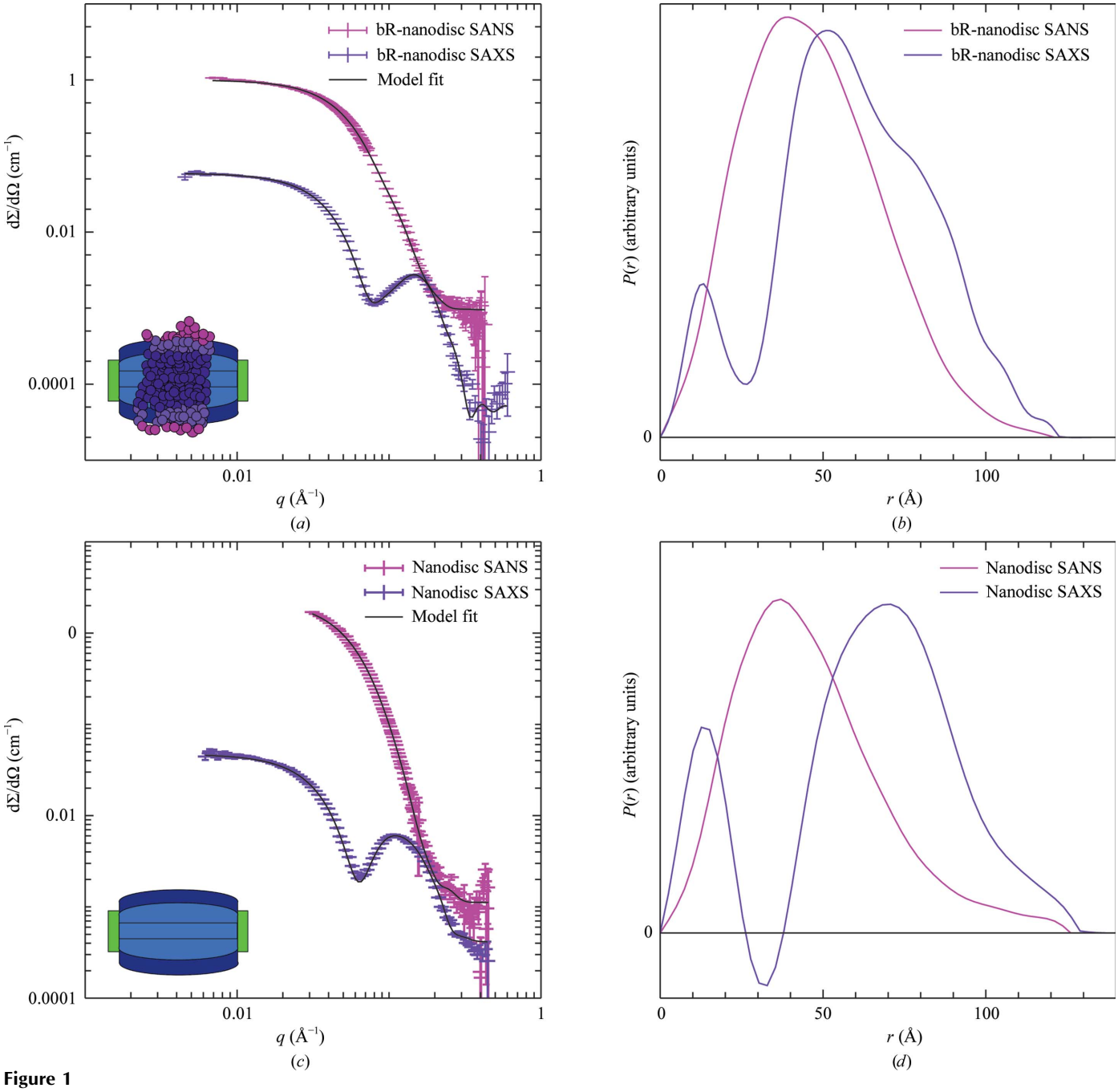


**Figure 1**
(*a*) SAXS (purple) and SANS (magenta) data from nanodiscs loaded with bR; model fits are shown in black. A buffer consisting of 100% $D_2O$ was used for the SANS measurements. (*b*) Pair-distance distribution functions corresponding to the scattering data in (*a*). (*c*) SAXS and SANS data from unloaded nanodiscs; model fits are shown as black lines. (*d*) Pair-distance distribution functions corresponding to the data shown in (*c*).

neutrons with a wavelength of 4.5 Å at three sample-to-detector distances: 1.27 m with 4 m collimation, 3.77 m with 4 m collimation and 7.77 m with 8 m collimation. These settings covered $q$-ranges of 0.035–0.45, 0.012–0.16 and 0.0057–0.077 $Å^{-1}$, respectively. Again, the wavelength spread was 10%.

Immediately before each scattering measurement, the 280 nm absorption of the samples was measured in order to determine the protein concentration using the extinction coefficients for bR and MSP given in Bayburt & Sligar (2003).

**2.1.6. Sample handling: SAXS**. The samples were thawed and spun at 12 000$g$ for 15 min in order to remove larger aggregates caused by freezing. Afterwards, the glycerol added as a cryoprotectant was removed by diluting the sample by a factor of ten and concentrating using a 50 kDa cutoff centrifuge filter. This was repeated an additional two times, giving a residual glycerol concentration of 0.00015%($v$/$v$); the final flowthrough was kept as an accurate buffer background for the SAXS measurements.

Sample handling was performed using the specialized sample-handling robot available at the BioSAXS beamline. A test run was performed in order to determine the exposure time of the sample before a measurable degree of radiation damage could be detected. Furthermore, the sample was flowed through the beam to make sure that the same volume of sample was not exposed twice. The sample was measured ten times for 500 ms during flow.

In order to obtain a precise buffer background, the flow-through from the spin filter was measured both before and after the sample and the average was used for subtraction.

**2.1.7. Sample handling: SANS**. To minimize the incoherent scattering from hydrogen, the Tris buffer was exchanged to Tris buffer prepared using $D_2O$ instead of $H_2O$. This greatly reduced the amount of hydrogen present in the sample and increased the scattering contrast of the protein and lipids in the sample. The buffer exchange was performed using a 50 kDa cutoff centrifuge filter; again, the sample was diluted by a factor of ten with the $D_2O$ buffer and concentrated back to the original concentration. This was repeated an additional two times, giving a residual $H_2O$ concentration of 0.001%($v$/$v$).

**2.1.8. Software and implementation**. The presented model was implemented in a larger data-analysis framework written in C and controlled *via* an interface written in Python. Using this framework, the model was fitted to the presented data with an adaptation of the Levenberg–Marquardt algorithm (Marquardt, 1963) using the so-called gridsearch implementation (Pedersen, 1997).

The minimization was cross-checked using the Broyden–Fletcher–Goldfarb–Shanno algorithm (Broyden, 1970; Fletcher, 1970; Goldfarb, 1970; Shanno, 1970) to ensure correctness and convergence. The source code for traditional implementations of these algorithms can be found in the literature (Press *et al.*, 1992).

Local minima are difficult to avoid in complex models. However, the inclusion of molecular constraints and the fitting on an absolute scale together with the condition that the model must fit SAXS and SANS data simultaneously significantly minimizes the number of truly different local minima as experienced in the model-fitting process.

Owing to the heavy nature of the computational tasks, parallelization was implemented using the OpenMP protocol for C, thereby expanding the calculation of $I(q)$ on the available CPUs. With these implementations, the time needed to compute the $\chi^2$ of a given model is a couple of seconds on a modern high-end desktop PC. Thus, execution of the entire minimization procedure takes from a couple of minutes to a couple of hours depending on the convergence criteria and the precision setup of the fitting routine as well as the initial parameter values for the model.

The mathematical tools used in the computation were based on the built-in routines in the mathematical library of C as well as the Gnu Scientific Library (GSL).

The presented confidence intervals were estimated using the profile-likelihood framework. The upper and lower bounds for each parameter were determined such that relaxation of the remaining parameters yields a fit with an increase in $\chi^2$ of no higher than 1.0, corresponding to the 68.3th percentile.

## 3. Theory and mathematical modelling

### 3.1. Development of a hybrid approach for structural modelling and analysis of data

For the data analysis, we have developed a novel general approach that combines the advantages of the two prevalent approaches used to analyze small-angle scattering data from particles in solution.

In the first of these approaches, which may be termed *continuous modelling*, particles are represented by simple geometrical objects and the spherical average of the analytical form-factor intensity is fitted to the data. Internal structure can be modelled by combining the form-factor amplitudes of various objects. These could, for instance, be concentric spheres of alternating scattering-length densitiy to account for the core-shell structure of detergent micelles (Cabane *et al.*, 1985). The particle form factors can be combined with analytical structure factors and size distributions, which allows the inclusion of concentration effects and polydispersity in the modelling. Analytic form factors are available for several shapes (Pedersen, 2002), and the approach has successfully been applied to describe a large number of systems, *e.g.* phospholipid vesicles (Kučerka *et al.*, 2010; Andersen *et al.*, 2011), detergent micelles (Lipfert *et al.*, 2007) and micro emulsions (Chen, 1986). Molecular constraints can easily be incorporated into the model, for example information about the molecular components and sample concentration.

The other approach, which may be termed *bead-based modelling*, has proved very successful in systems of monodisperse proteins in solution. Proteins may have complicated shapes but a relatively homogeneous scattering-length density on the relevant length scale. The method utilizes the fact that the scattering from an assembly of spherical beads can readily be calculated (Svergun & Koch, 2003). One bead can, for

instance, represent a single atom or an amino-acid residue. Examples of bead-based methods are *ab initio* and rigid-body modelling (Petoukhov & Svergun, 2005). In *ab initio* modelling, no prior knowledge of the shape of the protein is necessary. By moving one bead at a time, assuming homogeneous packing of the residues, a multitude of shapes can be explored. The overall shapes that fit the data are often strikingly similar and thus are likely to represent the actual shape of the protein (Svergun, 1999). If part of the protein has been crystallized, its residue positions can be determined from the crystal structure. This part is then treated as a rigid body that can be translated and rotated relative to the rest of the structure.

The hybrid approach proposed in the present work combines the two methods to allow a quick computation of the scattering from the nanodisc and membrane protein taking into account all of the *a priori* knowledge of the system. Fig. 2 illustrates how a dummy-residue model based on the crystal structure of a membrane protein is combined with a continuous model of the nanodisc within the hybrid approach. Various model parameters, such as the height of the lipid bilayer and the relative orientation of the membrane protein, can be varied to fit the experimental data.

In a previous study (Skar-Gislinge *et al.*, 2010; Skar-Gislinge & Arleth, 2010), it was shown that a nanodisc without a membrane protein could be described by the continuous approach. The disc was modelled as a set of concentric cylinders with elliptical cross-sections. The phospholipid bilayer consisted of three regions of different contrast representing lipid head-groups, lipid alkyl chains and lipid methyl groups, respectively. The MSP was modelled by an elliptical ring.

For the present work, we have used a slight modification of this model in which the head-group and alkyl-chain regions are slightly lens-shaped instead of flat (Kaya, 2004). This accounts for the possible effect of the lipids adjusting to the different hydrophobic heights of the MSP and the membrane protein. As described previously (Skar-Gislinge & Arleth, 2010), molecular constraints are systematically incorporated into the model to minimize the number of free parameters. The bacteriorhodopsin molecule is represented by point-like dummy residues. Each residue corresponds to one amino acid. Their relative positions are based on the coordinates of the crystal structure deposited in the PDB as entry 1py6 (Faham *et al.*, 2004). The position of each residue is determined by the centre of scattering of all of the atoms of that residue. For this calculation, it is taken into account that the position of the scattering centre depends on the scattering-length density of the displaced phase. The lateral position and rotation of the whole membrane protein relative to the nanodisc are the fitting parameters.

### 3.2. Computation of scattering from the hybrid model

The scattering amplitude from the membrane protein is combined with the description of the unloaded nanodisc in the following way: if the centre of mass of a residue is placed inside the lipid membrane in the nanodisc, the scattering from the displaced lipid (head group, alkyl chain or methyl group as appropriate) has to be subtracted, exactly as one usually subtracts scattering from displaced solvent. If the residue is outside the lipid membrane the scattering from the displaced solvent is instead subtracted.

In practice, the residue $j$ is weighted by its excess scattering length $\Delta b_j = b_j - \rho_j^{\rm bg} v_j$, where $b_j$ is its total scattering length and $v_j$ is its partial specific volume. The background $\rho_j^{\rm bg}$ is the scattering-length density of the displaced solvent if the residue is outside the lipid bilayer, or the excess scattering-length density $\Delta\rho_i$ of the appropriate part of the lipid if it is inside the

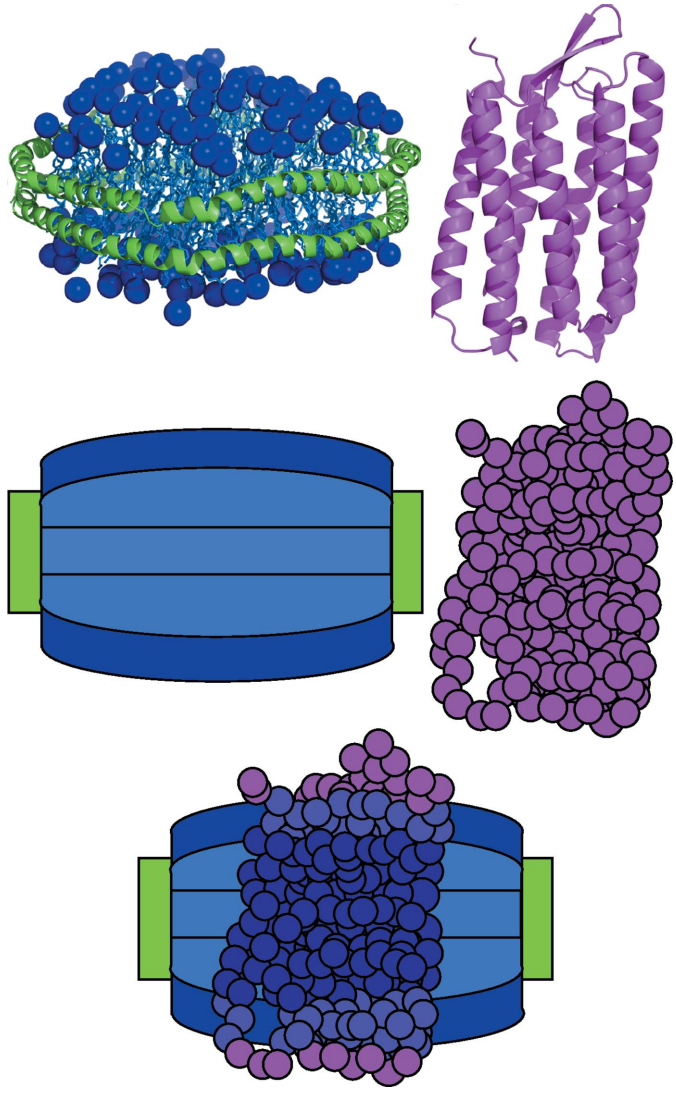

**Figure 2**
Top row: detailed atomic models from molecular dynamics (Shih *et al.*, 2005) of the unloaded nanodisc (left) and X-ray crystallography of bacteriorhodopsin (right). Middle row: simplified representations of the constituents corresponding to the level of resolution of small-angle scattering. The disc is represented by a few geometrical objects. The membrane protein is represented by a larger number of point-like dummy residues. Bottom: the simplified representations allow quick computation of the simulated scattering from the combined system. The different colours of the dummy residues signify that their weight factors have been adjusted to account for the displaced lipids.

bilayer. If the model membrane protein is translated relative to the membrane, some or all of the residues may move from one phase to another, for instance from the lipid head-group region to the solvent, and their excess scattering length must be adjusted accordingly.

In order to gain computational speed, the amplitudes of both the bead-based model of the membrane protein and the continuous description of the nanodisc are expanded in terms of spherical harmonics.

The spherical harmonic expansion coefficients, $A_{lm}$, of an assembly of $M$ beads is given by (Svergun *et al.*, 1995)

$$A_{lm}(q) = i^l \left(\frac{2}{\pi}\right)^{1/2} \sum_{j=1}^{M} \Delta b_j J_l(qr_j) Y^*_{lm}(\theta_j, \varphi_j). \quad (1)$$

The position of the $j$th bead in spherical coordinates is $\mathbf{r}_j = (r_j, \theta_j, \varphi_j)$. Its excess scattering length is given by $\Delta b_j$ as explained above. $J_l$ are the Bessel functions of the first kind and $Y^*_{lm}$ are the complex conjugates of the spherical harmonics.

On the other hand, the spherical harmonic expansion coefficients, $B_{lm}$, of the analytical form factor amplitudes, $F$, describing the continuous model of the unloaded nanodisc can be calculated by

$$B_{lm}(q) = \Delta b_{\rm nd} \left\langle F(\mathbf{q}) \frac{\exp(-im\beta)}{(2\pi)^{1/2}} \tilde{P}_{lm}[\cos(\alpha)] \right\rangle_{\alpha,\beta}, \quad (2)$$

where $\mathbf{q} = (q, \alpha, \beta)$ is the momentum-transfer vector in spherical coordinates, $\tilde{P}_{lm}$ are the Legendre polynomials and $\langle \ldots \rangle_{\alpha,\beta}$ denotes the spherical average. This is a double integral that has to be solved numerically.

The excess scattering length $\Delta b_{\rm nd}$ of the disc is given by $\Delta b_{\rm nd} = \sum_i V_i \Delta\rho_i$, where $V_i$ and $\Delta\rho_i$ are the volumes and excess length densities of the different phases, *e.g.* the lipid head group or MSP.

Even though the expansion (2) is computationally costly, this is compensated by the fact that the combined spherically averaged scattering intensity of the whole system, $I(q)$, can now easily be calculated by

$$I(q) = n \sum_{l=0}^{L} \sum_{m=-l}^{l} |A_{lm}(q) + B_{lm}(q)|^2. \quad (3)$$

The expression becomes exact for $L \rightarrow \infty$, but typically $L$ around 20 is sufficient. The intensity is proportional to the number density of scatterers $n$ and has units of scattering cross-section per unit volume.

Note that if the position of a single bead is changed, only one term in (1) and all of the terms of (3) need to be recalculated to obtain the scattering from the new configuration. This means that the scheme outlined here in principle allows *ab initio* modelling of proteins inside a lipid membrane in the case where a crystal structure is not available.

### 3.3. Model implementation

To fit the scattering data from bacteriorhodopsin incorporated into the nanodisc, the following parameters were adjusted. (i) The partial specific molecular volumes of the single lipids, the MSP and the membrane protein. These molecular volumes were not allowed to deviate more than a few percent from the pre-estimated values reported in the literature (Kučerka *et al.*, 2008; Skar-Gislinge *et al.*, 2010; Faham *et al.*, 2004; Fraser *et al.*, 1978). (ii) The height of the hydrophobic part of the lipid bilayer (at the rim) and the curvature of the bilayer. Together with the number of lipids in the disc, these parameters determine the cross-sectional area of the disc. (iii) The axis ratio of the elliptic cylinder representing the lipid bilayer was also taken as a fitting parameter, and thus the lengths of the major and minor axes of the elliptical cylinders constituting the lipid bilayer could be deduced. (iv) In addition, the number of hydration water molecules per lipid head group was fitted along with two roughness terms correcting for the fact that the interfaces are not perfectly smooth. These parameters are explained in more detail in a recent publication (Skar-Gislinge & Arleth, 2010). (v) The fitting parameters governing the positioning of the membrane protein were a vertical shift defined as the distance of the centre of mass of the membrane protein to the centre of the bilayer along the bilayer normal, a horizontal shift along the major semi-axis of the ellipsis and finally a tilt around the major semi-axis of the ellipsis of the main axis of the bR molecule relative to the surface normal of the lipid bilayer.

Hence, a total number of 13 free parameters were fitted. The model had to fit the SAXS curve and the SANS curve simultaneously, and the curves were fitted on an absolute scale. This meant that the total amount of excess scattering cross-section per unit volume from the electrons in the model had to add up to the forward scattering of the SAXS curve and at the same time the combined scattering cross-sections per unit volume of the nuclei had to add up to the forward scattering of the SANS curve. Some typical examples of excess scattering-length densities are given in Table 1. The excess scattering length, $\Delta b$, of an object of volume $V$ filled with a particular phase of contrast $\Delta\rho$ is $\Delta b = V\Delta\rho$. The forward scattering of a solution of particles that each have a total excess scattering length of $\Delta B$ is $n(\Delta B)^2$, where $n$ is the number of particles per unit volume of the solution.

## 4. Results

### 4.1. Visual inspection of SAXS and SANS data

The recorded two-dimensional scattering data were reduced and scaled as described in §2 and the appropriate backgrounds were subtracted. The background-subtracted SAXS and SANS data from nanodiscs with embedded bacteriorhodopsin are shown in Fig. 1 along with the corresponding indirect Fourier transforms (IFTs; Glatter, 1977). Also shown are the SAXS and SANS data sets of nanodiscs without incorporated bacteriorhodopsin.

The SAXS data of both the unloaded and loaded nanodiscs exhibit a characteristic minimum at around 0.08 Å$^{-1}$. This oscillatory behaviour is owing to the combination of positive and negative excess scattering-length densities characteristic of these phospholipid-based systems (see Table 1). While the oscillation is apparent both with and without the presence of

**Table 1**
Excess scattering-length densities for X-rays ($\Delta\rho_x$) and neutrons in 100% $D_2O$ ($\Delta\rho_n$).

For the lipid head groups the appropriate value for the 2:1 PC:PG mixture is given. The bR molecule is built from beads representing amino-acid residues with varying scattering contrast. The reported value is the weighted mean.

| | $\Delta\rho_x$ ($cm^{-2}$) | $\Delta\rho_n$ ($cm^{-2}$) |
|---|---|---|
| Lipids | | |
| Head group | $5.91 \times 10^{10}$ | $-3.66 \times 10^{10}$ |
| Alkyl chains | $-1.20 \times 10^{10}$ | $-6.60 \times 10^{10}$ |
| Methyl | $-4.73 \times 10^{10}$ | $-7.22 \times 10^{10}$ |
| Protein | | |
| bR (mean) | $3.94 \times 10^{10}$ | $-3.24 \times 10^{10}$ |
| MSP | $3.79 \times 10^{10}$ | $-2.88 \times 10^{10}$ |

bR, the specific shapes are clearly different in the two types of systems.

The oscillation is not seen in the SANS data since all of the constituents of the system have similar neutron contrasts on the background of 100% $D_2O$. This clearly shows that there is complementary information in the two data sets.

### 4.2. Pair-distance distribution functions

Indirect Fourier transformations were performed using the Bayesian indirect Fourier transformation method (BIFT; Hansen, 2000). Using Bayesian statistics, this method determines the pair-distance distribution function, $p(r)$, without prior user input, *e.g.* the maximum internal distance of the sample or the damping parameter (Glatter, 1977). This ensures that the $p(r)$ is obtained on a statistically sound basis without user bias. From the $p(r)$ functions, we see that the maximum distance within both the loaded and the unloaded nanodiscs is about 120 Å (see Fig. 1). The well defined maximum distances apparent from the $p(r)$ functions strongly confirm a high sample quality free of unintended large aggregates.

A further advantage of the BIFT method is that it provides a more reliable estimate of the experimental information content than the more commonly used number of Shannon channels (Vestergaard & Hansen, 2006). As part of this, the method provides an estimate of the so-called 'number of good parameters' present in the evaluated data set. This number gives a good estimate of the maximum number of independent model parameters that it is meaningful to fit to the experimental data.

The number of good parameters is calculated from the number of spline functions needed to describe a $p(r)$ function that gives a good fit to the data when the inverse Fourier transform is invoked. In this way, the quality of the data set is taken into account since fewer splines are necessary to fit a data set with large error bars.

From the BIFT analysis, the number of good parameters were calculated as $10.6 \pm 0.8$ in the SAXS data and $8.5 \pm 0.2$ in the SANS data.

The number of good parameters in the combined SAXS and SANS data set depends on the redundancy of the two measurements. If the contrast situations are similar, the information content will only be slightly improved by the second measurement. If the two situations are complementary the true number of free parameters may be as high as the sum of the numbers from the individual measurements. Unfortunately we have not found a way to formalize this, but it is safe to assume that in the data presented here the number of good parameters is significantly higher than 11 and is definitely smaller than 19.

From previous studies of the unloaded nanodisc, we found that the addition of another SANS contrast at the match point of the protein, *i.e.* 42% $D_2O$, only weakly constrains the fits.

### 4.3. Model-fit results

The data from the bR-loaded nanodiscs were fitted using (1), (2) and (3), whereas those from the unloaded nanodiscs were fitted using the previously published model of the

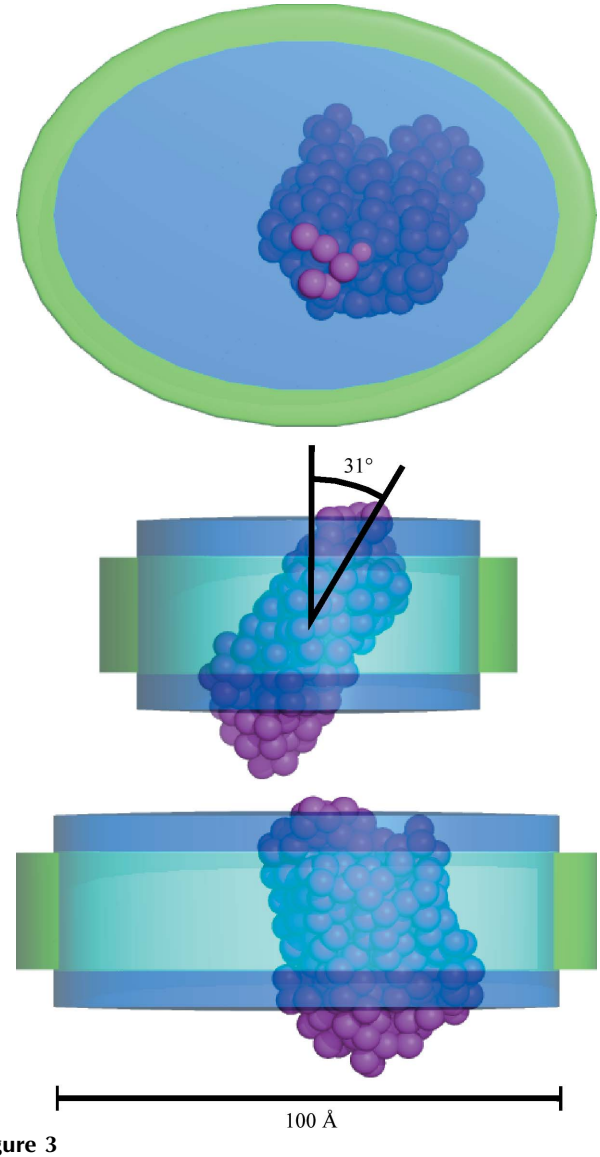


**Figure 3**
The best model fit to the data shown to scale viewed along the disc normal (top), major axis (middle) and minor axis (bottom). Green, membrane scaffolding protein (MSP). Cyan, hydrophobic part of the lipids. Blue, hydrophilic part of the lipids. Magenta, bacteriorhodopsin.

**Table 2**
Structural parameters from the model fits shown in Fig. 1.

A total number of 13 parameters were fitted to the data from the bR-carrying nanodisc and nine parameters were fitted to the unloaded nanodisc. The parameter marked (nf) was not fitted. The upper and lower bounds indicate the confidence interval corresponding to the 68.3rd percentile.

| | bR-loaded nanodisc | | | Unloaded nanodisc | | |
|---|---|---|---|---|---|---|
| | Lower bound | Fitted value | Upper bound | Lower bound | Fitted value | Upper bound |
| Fit parameters | | | | | | |
| bR tilt (°) | 23.1 | **31.2** | 42.6 | | — | |
| bR vertical shift (Å) | −7.0 | **−4.2** | 0 | | — | |
| bR horizontal shift (Å) | 10.4 | **12.1** | 13.3 | | — | |
| bR molecular volume (Å$^3$) | 32400 | **32900** | 33400 | | — | |
| Hydrophobic thickness at rim (Å) | 23.3 | **24.6** | 25.5 | 30.3 | **30.8** | 31.2 |
| Additional thickness at centre owing to curvature of bilayer (Å) | 0 | **1.8** | 6.44 | | 0 (nf) | |
| No. of lipids in disc | 128 | **130.6** | 133 | 125.7 | **126.66** | 127.9 |
| No. of bound $H_2O$ per lipid | 5.6 | **8.7** | 12.2 | 0 | **0** | 1.6 |
| Axis ratio of bilayer | 1.29 | **1.44** | 1.59 | 1.59 | **1.66** | 1.74 |
| Molecular volume per lipid (Å$^3$) | 1255 | **1261** | 1268 | 1280 | **1284** | 1288 |
| Molecular volume of one MSP (Å$^3$) | 26100 | **26500** | 26900 | 24600 | **25100** | 25400 |
| Interface roughness, X-rays (Å) | 5.4 | **5.58** | 5.9 | 5.08 | **5.36** | 5.67 |
| Interface roughness, neutrons (Å) | 5.0 | **5.32** | 5.7 | 4.41 | **4.56** | 4.73 |
| Radius of protruding His tags (Å) | | — | | 5.8 | **12.5** | 20.4 |
| Deduced parameters | | | | | | |
| Interface area per lipid (Å$^2$) | | 77.3 | | | 62.9 | |
| Bilayer thickness at rim (Å) | | 39.4 | | | 40.8 | |
| Bilayer thickness at centre (Å) | | 40.2 | | | 40.8 | |
| Bilayer circumference (Å) | | 272 | | | 234 | |

phospholipid nanodisc (Skar-Gislinge *et al.*, 2010; Skar-Gislinge & Arleth, 2010). The fit results are plotted together with the experimental data for both systems in Fig. 1 and the corresponding fit parameters are listed in Table 2. Note that each MSP has a protruding histidine tag. These were cleaved from the loaded nanodisc samples before measurement, while they remained on the unloaded nanodisc sample. The model takes this into account as described previously (Skar-Gislinge & Arleth, 2010).

We found that the bR molecule is significantly decentred in the nanodiscs but without touching the rim. The centre of mass of bR is displaced about 12 Å from the nanodisc centre (see Fig. 3), leaving room for a layer of about two phospholipids between the bR molecule and the membrane scaffolding protein. A significant tilt of bR is also observed when it is located in the nanodisc. The best model fit was obtained at a bR tilt angle of 31°. The tilt angle is defined to be zero when the mean directions of the seven transmembrane helices points in the direction of the bilayer normal. The vertical position of the bR molecule is close to centred, and the best model fit was found, when the centre of mass was displaced by −4.2 Å along the bilayer normal with respect to the bilayer centre.

The number of bound water molecules at the head groups is difficult to determine using this method. This is reflected by the large confidence intervals. The fitted number of 8.7 water molecules per head group for the bR-loaded nanodisc is surprisingly high. On the other hand, zero bound water molecules in the unloaded nanodisc appears to be unrealistically low.

Owing to the high degree of symmetry of bacteriorhodopsin, it was possible to find alternative solutions with tilt angles of approximately 31° and/or a positive lateral shift. However, taking the polarity of the surface residues into account these solutions are unlikely, and we conclude that it is the region containing the C-terminus that protrudes the most, while the region around the N-terminus is partly buried in the hydrophilic head groups of the bilayer. As an example, Fig. 4 shows the most likely solution together with an alternative solution with a positive lateral shift. The amino acids are coloured according to their hydrophobicity on the Wimley–White scale (Wimley & White, 1996). The alternative solution has been deemed to be less plausible owing to a larger number of charged amino-acid residues extending into the solvent and a similar increase in the number of aromatic residues residing inside the hydrophobic core of the lipid bilayer. Furthermore, the high curvature of the bilayer leads to a large hydrophobic mismatch between the height of the MSP and the height of the hydrophobic core. Except for the sign of the vertical shift and the hydrophobic thickness at the rim, the parameters of the alternative solution all fall within the confidence intervals given in Table 2.

The presence of bR perturbs the surrounding nanodisc significantly. This is observed in the axis ratio of the discs, with a decrease from 1.66 to 1.44, and more notably in the hydrophobic interface area per lipid, where a significant change from 62.6 Å$^2$ in the unloaded discs to 78.4 Å$^2$ in the bR-loaded discs is observed. Surprisingly, the introduction of bR does not appear to displace any of the lipids. Instead, the fitted number of lipids increases from 126 in the unloaded disc to 130 in the bR-loaded disc. The combined result of these effects is a quite significant increase in the circumference of the disc from 238 Å in the unloaded disc to 275 Å in the loaded disc, an increase of 16%. While it was surprising to us that the MSP exhibits this flexibility, it is noted that the circumference of the loaded disc corresponds well to the expected maximal length of the helices constituting the MSP.

## 5. Discussion

Our method gives unique experimental insight into how a membrane protein is organized in a lipid-membrane environment, including how the lipids themselves adapt structurally to accommodate the membrane protein. This gives us the opportunity to test some of the many theoretical predictions and computer simulations of these interactions (Lomize *et al.*, 2011; Mouritsen & Bloom, 1984; Israelachvili *et al.*, 1980).

From a visual inspection of the crystal structure of bacteriorhodopsin based on the polarity of the surface residues, one

would estimate the hydrophobic height to be 35 Å (Lee, 2003). On the other hand, the height of the hydrophobic part of an unstretched bilayer of POPC has been measured to be 27.1 Å using X-ray diffraction (Kučerka *et al.*, 2008). Finally, the hydrophobic height of the MSP is estimated to be 24 Å.

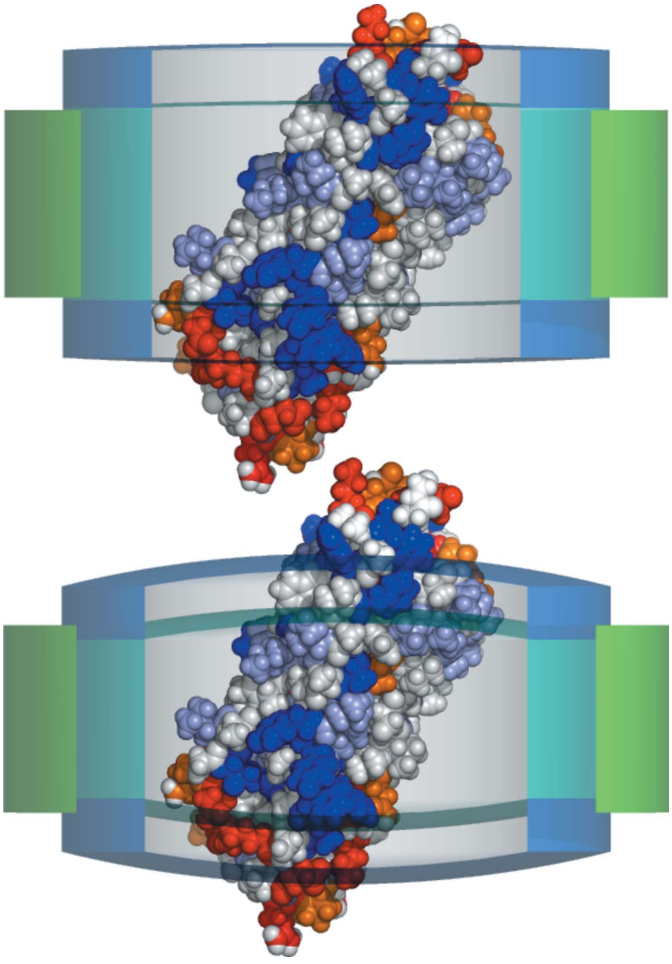

**Figure 4**
Top, the solution shown in Figs. 2 and 3. Bottom, an alternative solution giving an equally good fit to the data but a less favourable hydrophobic match. Blue, charged hydrophobic residues. Light blue, slightly hydrophobic residues. Orange, slightly hydrophilic residues. Red, aromatic hydrophilic residues.

To account for this mismatch, the lipids may alter their hydrophobic height by stretching or compressing and a membrane protein may lower its hydrophobic height by tilting such that none of the transmembrane segments penetrate the membrane perpendicularly. Finally, in some situations it may be thermodynamically favourable to settle for a conformation with a slight hydrophobic mismatch. The present work is to our knowledge the first experimental quantification of the interplay between all these effects.

In this work, we clearly see how bR tilts to accommodate the mismatch of the hydrophobic heights. While we had anticipated that the lipids would stretch to cover the hydrophobic parts of bR, we observe the opposite behaviour. This may be the result of an outwards pressure on the MSP owing to a less structured packing of the lipids caused by the presence of bR. Thereby, the MSP loses flexibility and its hydrophobic height comes close to the 24 Å expected from two parallel helical segments. In a competition where the bilayer is compressed at the rim and stretched near the centre, the MSP is likely to have the largest effect because the rim is much longer than the circumference of the membrane protein (see Fig. 5).

In the same context, we observe that the bR molecule is significantly decentred in the nanodisc. Whether this observation is owing to the protein being fixed near the rim owing to more optimal lipid-bilayer packing in this region or owing to a lack of confinement of the protein position, we cannot say from the data. However, it is interesting to observe that the centre position is definitely not preferred by the membrane protein.

It is very interesting to compare the above results with the theoretical predictions deposited in the Orientation of Proteins in Membranes (OPM) database (Lomize *et al.*, 2011), which contains calculations of optimum lateral position and tilt angle as well as ideal bilayer thickness for most of the crystallized membrane proteins in the PDB. These calculations seek to minimize the transfer energy of the residues from water to the lipid bilayer, represented by a planar slab of adjustable thickness (Lomize *et al.*, 2006). As seen in Table 3, the tilt and lateral shift are comparable, whereas we observe a slightly lower hydrophobic thickness than the theoretical optimum predicted by the OPM. The differences may arise

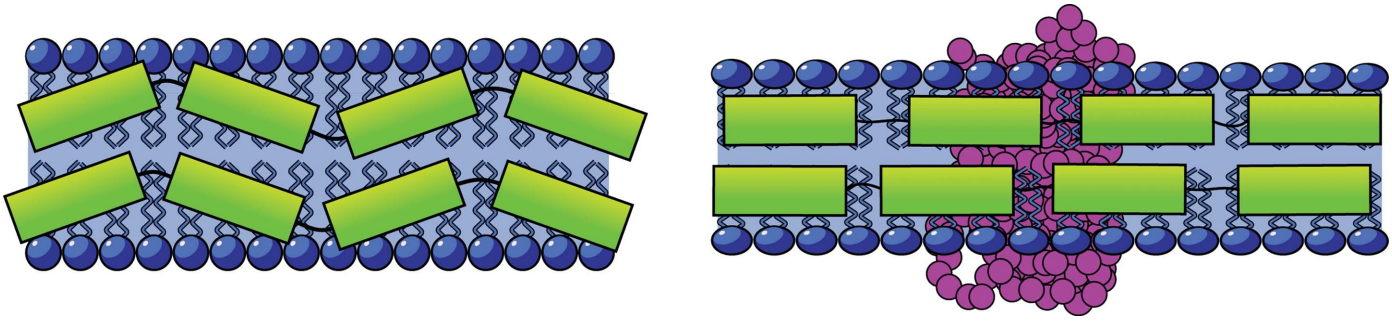

**Figure 5**
The loaded nanodisc (right) has a larger circumference than the unloaded nanodisc (left). This is a combined effect of the facts that more material has to fit inside the MSP (*i.e.* slightly more lipids plus the membrane protein) and that each lipid has an increased interface area. The sketch illustrates how the latter effect is self-amplifying because the lipids are perturbed by the stretched MSP of the loaded disc.

**Table 3**
Comparison of theoretical results from the Orientation of Membrane Proteins (OMP) database (Lomize *et al.*, 2011) and experimental results from this work.

| | Tilt (°) | Lateral shift (Å) | Hydrophobic thickness (Å) |
|---|---|---|---|
| OPM | 24 ± 8 | −3.3 | 29.6 ± 2.2 |
| This work | 31 | −4.2 | 26.4 (centre) |

from the fact that the bilayer of the nanodisc is not a naturally relaxed membrane.

A few experimental studies exist that reveal structural information about proteins in membranes. In particular, bR has been investigated (Altenbach *et al.*, 1990, 1994; Dumas *et al.*, 1999). For example, experiments in which residues in the fourth $\alpha$-helix (residues 103–129) of bR have been systematically replaced with spin-labelled cysteines have given insight into the depth of the residues in the lipid bilayer (Altenbach *et al.*, 1994). According to this study, residue Ile117 is centred in the bilayer. This method relies on the fact that no native cysteines are present in bR and that the mutant folds in the same way as the native protein. In the present work the lateral position of the residue Ile117 in the best fit to data is 0.6 Å relative to the centre of the bilayer, which is in excellent agreement with the spin-labelling study.

Lipid-bilayer thickness has been estimated by investigating changes in melting temperature owing to the incorporation of membrane proteins in lipid vesicles. Data for bR show that a positive shift in melting temperatures is observed for di(C12:0)PC, whereas a negative shift of comparable size is seen for di(C18:0)PC (Piknová *et al.*, 1993). This indicates that the hydrophobic matching of bR is achieved at chain lengths of around 30 Å. This is midway between the average chain lengths of the two lipid types. The slightly lens-shaped bilayer with hydrophobic height between 24.6 and 26.4 Å obtained in this study is only partly comparable to the result of the phase-transition study and the OPM value. This is because the lipid bilayer of the nanodisc is constrained at the rim by the MSP to a thickness of only 24 Å. This is less than most membrane proteins and has the effect that the bilayer becomes stretched like the head of a drum. The high degree of stress on the phospholipids may explain some of the difficulties in reconstituting certain membrane proteins in the nanodiscs. It would be interesting to investigate whether or not this could be resolved by using a mixture of lipids with different chain lengths.

### 5.1. Perspectives

At present, the primary bottleneck of the method is the difficulty in obtaining pure and well defined samples of reconstituted membrane proteins in sufficient amounts to allow both SAXS and SANS measurements. Assuming this can be solved, systems of interest can be grouped into two cases depending on whether or not *a priori* knowledge of the protein is present in the form of a crystal structure.

The presented approach is directly applicable in its present form to determine the localization of any membrane protein in the bilayer membrane of the nanodisc provided that the crystal structure is known. In cases where only extracellular parts have been crystallized, this could, with little effort, be combined with a good hypothesis of the membrane part and allow determination of the position and the orientation of the extracellular parts. Furthermore, it is trivial to generalize the approach to other systems in which the membrane protein is incorporated into other carrier systems, for example detergent micelles or lipid-bilayer vesicles.

For cases in which the membrane-protein structure is not known, it is the goal of our efforts to develop a free-form modelling approach comparable to the methods implemented in software such as *DAMMIN* and *GASBOR* (Svergun & Koch, 2003).

In this approach, each amino-acid residue moves freely and thus the model has hundreds of free parameters. Although we cannot hope for a unique solution, the packing constraints of the residues, such as nearest-neighbour distances, inherent to all proteins together with scattering data may be sufficient to determine the overall shape of the membrane protein. In the present case, we find that a little more experimental information is needed for this approach to be successful.

In order to obtain this, it may be advantageous to deuterate the MSP such that the MSP and the membrane protein do not have the same scattering-length density when investigated using neutrons. An even more optimal approach that we are currently investigating is to systematically control the deuteration levels of the MSP and the phospholipids (head groups and alkyl chains) to completely match the surrounding nanodisc carrier in the SANS experiment.

It is also relevant to further investigate the possibility of including other types of information. We already routinely include molecular constraints, *i.e.* information about the sample concentration, chemical composition and scattering length of the constituents, as well as partial specific molecular volumes. In this work, we have shown how this can be combined with structural information from crystallography. However, other structural methods such as cryo-EM might also provide useful constraints. It might also be possible to include local structure information from spectroscopic methods such as NMR, CD and others. Finally, general bioinformatical knowledge, including the packing density of the residues, could be systematically incorporated.

In order to make use of the improving resolution at high $q$ at modern SAXS and SANS facilities, we are working to introduce realistic local structure on a length scale of nanometres in the nanodisc model to allow close fitting at high $q$. This may be performed by incorporating information about the internal structure of lipids and MSP. Under all circumstances, we envisage a continuous demand for access to combined X-ray and neutron experiments as well as the possibility of increasingly small sample volumes.

## 6. Conclusion

We have presented a method to determine the position and orientation of a membrane protein relative to a phospholipid

nanodisc. For the specific case of bacteriorhodopsin (bR), we find that bR is displaced by 4.2 Å in the direction perpendicular to the lipid bilayer of the nanodisc. We find that bR is not confined to the centre of the disc but is more likely to be found 12 Å from the centre of the disc. The method also allows us to determine the response of the lipid bilayer. In the investigated case we observe a larger disc perimeter and a larger area per head group of the lipid molecules relative to an unloaded nanodisc. The method is applicable to other systems of membrane proteins embedded into a nanodisc.

The authors gratefully acknowledge the access to large-scale facility SANS and SAXS beamtime at the SANS beamline D11, Institute Laue–Langevin (ILL), at the BM29 (formerly ID14-3) Bio-SAXS beamline, European Synchrotron Radiation Facility (ESRF) and at KWS 1, Forschungs Neutronenquelle Heinz Maier-Leibnitz, Munich (FRM II). In this context, we gratefully acknowledge the access to simultaneous SAXS and SANS beamtime at ILL and ESRF. In addition, the authors thank Dr A. Round at ESRF and Dr H. Frielinghaus at FRM II. The authors also thank B. Justesen for preparation of the unloaded nanodisc samples. The UNIK synthetic biology project and McXtrace are gratefully acknowledged for cofunding of this research.

## References


Altenbach, C., Greenhalgh, D. A., Khorana, H. G. & Hubbell, W. L. (1994). *Proc. Natl. Acad. Sci. USA*, **91**, 1667–1671.

Altenbach, C., Matri, T., Khorona, H. G. & Hubbell, W. L. (1990). *Science*, **248**, 1088–1092.

Andersen, H. D., Wang, C., Arleth, L., Peters, G. H. & Westh, P. (2011). *Proc. Natl. Acad. Sci. USA*, **108**, 1874–1878.

Baas, B. J., Denisov, I. G. & Sligar, S. G. (2004). *Arch. Biochem. Biophys.* **430**, 218–228.

Bayburt, T. H., Grinkova, Y. V. & Sligar, S. G. (2002). *Nano Lett.* **2**, 853–856.

Bayburt, T. H., Grinkova, Y. V. & Sligar, S. G. (2006). *Arch. Biochem. Biophys.* **450**, 215–222.

Bayburt, T. H. & Sligar, S. G. (2003). *Protein Sci.* **12**, 2476–2481.

Berthaud, A., Manzi, J., Pérez, J. & Mangenot, S. (2012). *J. Am. Chem. Soc.* **134**, 10080–10088.

Broyden, C. G. (1970). *IMA J. Appl. Math. Med. Biol.* **6**, 76–90.

Cabane, B., Duplessix, R. & Zemb, T. (1985). *J. Phys.* **46**, 2161–2178.

Calcutta, A., Jessen, C. M., Behrens, M. A., Oliviera, C. L. P., Renart, M. L., González-Ros, J. M., Pedersen, J. S. & Malmedal, A. (2012). *Biochim. Biophys. Acta*, **1818**, 2290–2301.

Chen, S. (1986). *Annu. Rev. Phys. Chem.* **37**, 351–399.

Dencher, N. (1982). *Methods Enzymol.* **88**, 5–10.

Dumas, F., Lebrun, M. C. & Tocanne, J.-F. (1999). *FEBS Lett.* **458**, 271–277.

El Moustaine, D., Granier, S., Doumazane, E., Scholler, P., Rahmeh, R., Bron, P., Mouillac, B., Banères, J.-L., Rondard, P. & Pin, J.-P. (2012). *Proc. Natl. Acad. Sci. USA*, **109**, 16342–16347.

Fagerberg, L., Jonasson, K., von Heijne, G., Uhlén, M. & Berglund, L. (2010). *Proteomics*, **10**, 1141–1149.

Faham, S., Yang, D., Bare, E., Yohannan, S., Whitelegge, J. P. & Bowie, J. U. (2004). *J. Mol. Biol.* **335**, 297–305.

Fletcher, R. (1970). *Comput. J.* **13**, 317–322.

Fraser, R. D. B., MacRae, T. P. & Suzuki, E. (1978). *J. Appl. Cryst.* **11**, 693–694.

Frauenfeld, J., Gumbart, J., van der Sluis, E. O., Funes, S., Gartmann, M., Beatrix, B., Mielke, T., Berninghausen, O., Becker, T., Schulten, K. & Beckmann, R. (2011). *Nature Struct. Mol. Biol.* **18**, 614–621.

Glatter, O. (1977). *J. Appl. Cryst.* **10**, 415–421.

Goldfarb, D. (1970). *Math. Comput.* **24**, 23–26.

Gonen, T., Cheng, Y., Sliz, P., Hiroaki, Y., Fujiyoshi, Y., Harrison, S. C. & Walz, T. (2005). *Nature (London)*, **438**, 633–638.

Green, N. (1970). *Methods Enzymol.* **18**, 418–424.

Hagn, F., Etzkorn, M., Raschle, T. & Wagner, G. (2013). *J. Am. Chem. Soc.* **135**, 1919–1925.

Hansen, S. (2000). *J. Appl. Cryst.* **33**, 1415–1421.

Israelachvili, J. N., Marcelja, S. & Horn, R. G. (1980). *Q. Rev. Biophys.* **13**, 121–200.

Kaya, H. (2004). *J. Appl. Cryst.* **37**, 223–230.

Kučerka, N., Nagle, J. F., Sachs, J. N., Feller, S. E., Pencer, J., Jackson, A. & Katsaras, J. (2008). *Biophys. J.* **95**, 2356–2367.

Kučerka, N., Nieh, M. & Katsaras, J. (2010). *Advances in Planar Lipid Bilayers and Liposomes*, Vol. 12, edited by A. Iglič, ch. 4. Oxford: Academic Press.

Lee, A. (2003). *Biochim. Biophys. Acta*, **1612**, 1–40.

Lieutenant, K., Lindner, P. & Gahler, R. (2007). *J. Appl. Cryst.* **40**, 1056–1063.

Lipfert, J., Columbus, L., Chu, V. B., Lesley, S. A. & Doniach, S. (2007). *J. Phys. Chem. B*, **111**, 12427–12438.

Lomize, A. L., Pogozheva, I. D. & Mosberg, H. I. (2011). *J. Chem. Inf. Model.* **51**, 930–946.

Lomize, M. A., Lomize, A. L., Pogozheva, I. D. & Mosberg, H. I. (2006). *Bioinformatics*, **22**, 623–625.

Lyukmanova, E. N., Shenkarev, Z. O., Khabibullina, N. F., Kopeina, G. S., Shulepko, M. A., Paramonov, A. S., Mineev, K. S., Tikhonov, R. V., Shingarova, L. N., Petrovskaya, L. E., Dolgikh, D. A., Arseniev, A. S. & Kirpichnikov, M. P. (2012). *Biochim. Biophys. Acta*, **1818**, 349–358.

Marquardt, D. (1963). *J. Soc. Ind. Appl. Math.* **11**, 431–441.

Morth, J. P., Pedersen, B. P., Toustrup-Jensen, M. S., Sørensen, T. L.-M., Petersen, J., Andersen, J. P., Vilsen, B. & Nissen, P. (2007). *Nature (London)*, **450**, 1043–1049.

Mouritsen, O. & Bloom, M. (1984). *Biophys. J.* **46**, 141–153.

Mylonas, E. & Svergun, D. I. (2007). *J. Appl. Cryst.* **40**, s245–s249.

Oesterhelt, D. & Stoeckenius, W. (1974). *Methods Enzymol.* **31**, 667–678.

Pedersen, J. S. (1997). *Adv. Colloid Interface Sci.* **70**, 171–210.

Pedersen, J. S. (2002). *Neutrons, X-rays and Light: Scattering Methods Applied to Soft Condensed Matter*, edited by P. Linder & T. Zemb, ch. 16. Amsterdam: Elsevier.

Periasamy, A., Shadiac, N., Amalraj, A., Garajová, S., Nagarajan, Y., Waters, S., Mertens, H. D. T. & Hrmova, M. (2013). *Biochim. Biophys. Acta*, **1828**, 743–757.

Pernot, P., Theveneau, P., Giraud, T., Fernandes, R. N., Nurizzo, D., Spruce, D., Surr, J., McSweeney, S., Round, A., Felisaz, F., Foedinger, L., Gobbo, A., Huet, J., Villard, C. & Cipriani, F. (2010). *J. Phys. Conf. Ser.* **247**, 012009.

Petoukhov, M. V. & Svergun, D. I. (2005). *Biophys. J.* **89**, 1237–1250.

Piknová, B., Páerochon, E. & Tocanne, J.-F. (1993). *Eur. J. Biochem.* **218**, 385–396.

Press, W. H., Teukolsky, S. A., Vettering, W. T. & Flannery, B. P. (1992). *Numerical Recipes in C. The Art of Scientific Computing*, 2nd ed. Cambridge University Press.

Ritchie, T. K., Grinkova, Y. V., Bayburt, T. H., Denisov, I. G., Zolnerciks, J. K., Atkins, W. M. & Sligar, S. G. (2009). *Methods Enzymol.* **464**, 211–231.

Rosenbaum, D. M., Rasmussen, S. G. F. & Kobilka, B. K. (2009). *Nature (London)*, **459**, 356–363.

Shanno, D. F. (1970). *Math. Comput.* **24**, 647–656.

Shih, A. Y., Denisov, I. G., Phillips, J. C., Sligar, S. G. & Schulten, K. (2005). *Biophys. J.* **88**, 548–556.

Skar-Gislinge, N. & Arleth, L. (2010). *Phys. Chem. Chem. Phys.* **13**, 3161–3170.

Skar-Gislinge, N., Simonsen, J. B., Mortensen, K., Feidenhans'l, R., Sligar, S. G., Lindberg Møller, B., Bjørnholm, T. & Arleth, L. (2010). *J. Am. Chem. Soc.* **132**, 13713–13722.

Sonntag, Y., Musgaard, M., Olesen, C., Schiøtt, B., Møller, J. V., Nissen, P. & Thøgersen, L. (2011). *Nature Commun.* **2**, 304.
Svergun, D. I. (1999). *Biophys. J.* **76**, 2879–2886.
Svergun, D., Barberato, C. & Koch, M. H. J. (1995). *J. Appl. Cryst.* **28**, 768–773.
Svergun, D. I. & Koch, M. H. J. (2003). *Rep. Prog. Phys.* **66**, 1735–1782.
Vestergaard, B. & Hansen, S. (2006). *J. Appl. Cryst.* **39**, 797–804.
Wallin, E. & von Heijne, G. (1998). *Protein Sci.* **7**, 1029–1038.
Whorton, M. R., Bokoch, M. P., Rasmussen, S. G. F., Huang, B., Zare, R. N., Kobilka, B. & Sunahara, R. K. (2007). *Proc. Natl. Acad. Sci. USA*, **104**, 7682–7687.
Wimley, W. C. & White, S. H. (1996). *Nature Struct. Mol. Biol.* **3**, 842–848.
Yao, X. J., Vélez Ruiz, G., Whorton, M. R., Rasmussen, S. G. F., Devree, B. T., Deupi, X., Sunahara, R. K. & Kobilka, B. (2009). *Proc. Natl. Acad. Sci. USA*, **106**, 9501–9506.